Analytica Chimica Acta 1084 (2019) 71–77

Contents lists available at ScienceDirect

Analytica Chimica Acta

journal homepage: www.elsevier.com/locate/aca

Plasmonic nanobiosensor based on Au nanorods with improved sensitivity: A comparative study for two different configurations

Linus Pauling F. Peixoto [a], Jacqueline F.L. Santos [b, **], Gustavo F.S. Andrade [a, *]

[a] Laboratório de Nanoestruturas Plasmônicas, Núcleo de Espectroscopia e Estrutura Molecular, Centro de Estudos em Materiais, Departamento de Química, Universidade Federal de Juiz de Fora, 36036-900, Juiz De Fora, MG, Brazil
[b] Laboratório de Materiais Aplicados e Interfaces, Instituto de Química, Universidade Federal do Rio Grande do Sul, Porto Alegre, RS, Brazil

HIGHLIGHTS

- Biosensors based on Au nanorods suitable for two different approaches were developed.
- The sensitivity and figure-of-merit for LSPR are at least 18% and 114% superior to that reported before.
- Both substrates were submitted to proof-of-concept experiments for biosensing of anti-BSA performing satisfactorily.
- This study presents a step toward optimization of Au anisotropic nanoparticles LSPR biosensors.
- This biosensor presents a simple methodology and short time of analysis.

GRAPHICAL ABSTRACT

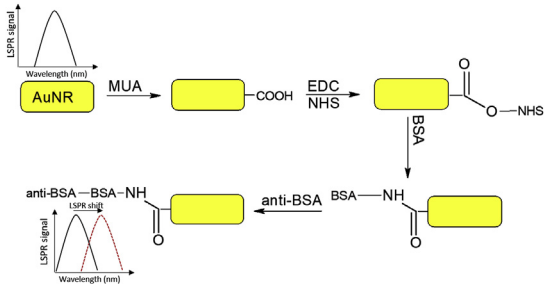

ARTICLE INFO

Article history:
Received 26 March 2019
Received in revised form
15 July 2019
Accepted 18 July 2019
Available online 20 July 2019

Keywords:
Plasmonic
Biosensors
LSPR
Solution-phase LSPR biosensor
Chip LSPR biosensor
Gold nanorods

ABSTRACT

Biosensors presenting high sensitivity for the detection of biomolecules are very promising for diseases diagnosis. Nowadays, there is a need for the development of biosensors with fast, trustworthy diagnosis and mostly with low cost, mainly for applications in developing countries. Label-free plasmonic biosensors are good candidates to reach out all these characteristics due to the possibility of spectral tunability, fast sensor response, real-time detection, strong enhancement of the local electric field and excellent adaptability to assemble different nanobiotechnology architectures. In this paper, two different configurations for LSPR based biosensor were developed by using solution-phase gold nanorods (S—P-AuNRs) and AuNRs-chip. The LSPR sensitivities were evaluated by monitoring shifts in the longitudinal plasmon band with changes in the refractive index of the medium surrounding the nanoparticles. AuNRs-chip presented higher sensitivity of 297 nm RIU^{-1} (refractive index unit) against 196 nm RIU^{-1} for S—P-AuNRs. Figure of merit (FOM) for AuNRs-chip and S—P-AuNRs were 3.0 and 2.2 RIU^{-1}, respectively. This result was assigned to the coupling of the lower energy longitudinal LSPR mode of propagation for AuNRs-chip among nearby nanoparticles in the film. In addition, an improvement of at least 18% in sensitivity was obtained comparing to others AuNRs based assay with similar aspect ratio. FOM is more appropriate to compare different approaches, in this case, the proposed biosensor reached improvements of at least 114%, presenting higher values even when compared to AuNRs of higher aspect ratio. As a proof of concept, AuNRs surface was chemically modified using mercaptoundecanoic acid followed activation

* Corresponding author.
** Corresponding author.
E-mail addresses: jacqueline.ferreira@ufrgs.br (J.F.L. Santos), gustavo.andrade@ufjf.edu.br (G.F.S. Andrade).

https://doi.org/10.1016/j.aca.2019.07.032

with ethylcarbodiimide and N-hidroxysuccinimide to allow the interaction between Bovine Serum Albumin (BSA) antibody and correspondent antigen. Both configurations studied resulted in efficient plasmonic biosensors, presenting high sensitivity for changes in the refractive index and for surface binding with anti-BSA.

1. Introduction

The collective electronic oscillation of metallic surfaces excited by electromagnetic radiation are denominated Surface Plasmons (SP) and when the size of this metallic objects is smaller or comparable to the incidence wavelength, the SP are referred to as localized. Resonance happens for the excitation wavelength that matches the oscillations modes of surface electrons [1], and then it may be called Localized Surface Plasmon Resonance (LSPR) [2]. LSPR is observed in different nanostructures, but for coinage metals (Au, Ag and Cu), is easily observed in the visible. Nanostructures supporting LSPR may present extremely intense and localized electromagnetic field in the vicinity of their surface. The properties of LSPR are highly dependent on the material, size and shape of the metallic nanoparticles involved due to changes in the surface polarizability [3]. Actually, the LSPR wavelength can be conveniently tuned throughout the visible, near-infrared and infrared region, presenting extremely intense and localized electromagnetic field in the vicinity of their surface, which is dependent of the refractive index of the local dielectric environment around the nanostructure [4]. This property has been extensively explored in the application of biosensors [5].

Plasmonic biosensors, on the other hand, are analytical tools that use the LSPR phenomenon to obtain a biological response based on interaction of the analyte to modified plasmonic metal surface and convert this response to an analytical signal based on measurable shifts of the position of the plasmonic resonance caused by the analyte. LSPR sensors have been intensively studied for healthcare, clinic treatments and real-time diagnostics [4]. It is well known that biosensor devices are composed by a bioreceptor that recognizes the analyte, which is also essential of LSPR biosensors, and specifically for immunoassays, the interaction antigen-antibody is used for the molecular recognition [6].

There are several shapes of metallic nanoparticles obtained through advanced synthetic methods for application in biosensors [7,8]. Gold nanoparticles for example have a simple surface chemistry and they are relatively bio-inert particles, promoting these nanostructures as good substrate for biomedical applications, including biomolecules detection [9], however gold nanorods (AuNRs) present the advantage of enabling to modulate the LSPR properties by controlling the aspect ratio during the synthesis [10], leading to improvements in the sensitivity due to the lower energy of the longitudinal plasmonic mode [11]. It is possible to use different configurations for AuNRs based biosensors, resulting for example in chip, optical fiber or solution-phase (S–P) based LSPR biosensor [4,12]. Their difference consists in which the sensor can be configured by either adsorbing the nanoparticles on a transparent substrate or just by simply leaving functionalized nanoparticles suspended in the solution. A variety of methodologies of synthesis and configurations of the sensor allowed the development of AuNRs-based LSPR biosensors with sensitivities and FOM (figure of merit) of 170–366 nm RIU^{-1} (refractive index unit) and 1.3–1.7 RIU^{-1}, respectively [5,13,14].

The diversity of sensors and detection systems available nowadays indicate that plasmonic biosensors come to light as a great solution for a huge range of biochemical and biomedical problems [15]. For example, plasmonic biosensors can be applied in systems spanning from detection of a protein-protein interaction up to DNA fragments and detection at attomolar concentrations [16], allowing the analysis of real samples of food, cosmetics and biological fluids for example [17–20]. Indeed, the LSPR-based biosensing is an interesting proposal for new diagnostic procedures in developing economies, because the costs may be reduced with rational design, while keeping high effectiveness as biosensors [21]. Presently, the miniaturization, automation and smartphone based diagnostics devices are considered a frontier in biomedicine, which resulted in a driving force in the development of LSPR-based biosensors research [22–24].

Although the consistent research on LSPR based biosensor, there are some issues concerning the reproducibility and control of the aspect ratio during the production of AuNRs from seed mediated growth. AuNRs presenting shorter full width at half maximum would present better biosensor performance, quantified by the FOM values. Therefore, aiming to obtain a cost effective AuNRs based LSPR biosensor with improved sensitivity, we report a simple methodology to obtain AuNRs-based label free immunobiosensor in two different configurations: S–P-AuNRs biosensor, where AuNRs were in colloidal suspensions and AuNRs chip-biosensor, where AuNRs were chemically adsorbed on glass substrates. The AuNRs-chip was constructed with an improved immobilization method, which increases the density of AuNRs adsorbed and consequently the biosensor performance. Both configurations had their efficiencies as biosensor compared with previous methodologies in the literature through sensitivity measurements and a proof-of-concept immunoassay was done using the widely known antigen–antibody interaction between BSA and anti-BSA [25].

2. Material and methods

2.1. Material

Cetiltrimethylammonium bromide (CTAB), Sodium borohydride, N-hydroxisuccinimide (NHS) were purchased from Fluka and used without further purification. Tetrachloroauric acid, Silver nitrate, 11-mercaptoundecanoic acid (MUA), N-ethyl-N-(3-dietilaminepropyl carbodiimide) (EDC), 3-mercaptopropyl-trimethoxysilane (MPTMS), bovine serum albumin (BSA), bovine serum albumin antibody (anti-BSA) were purchase from Sigma-Aldrich and used without further purification. Aqueous solutions were prepared using deionized water (R = 18.2 MΩ cm) from a Millipore Synergy unity.

2.2. Equipment

The UV–Vis spectra of S–P-AuNRs and AuNRs-chip were acquired with an Ocean Optics Fiber spectrometer USB2000 or USB2000+, equipped with a visible light source (400–1100 nm) or ultraviolet and visible light source (200–1100 nm). The refractive indexes of the solutions were obtained in an Abbè refractometer. The centrifugation was performed in an Eppendorf Centrifuge 5418.

Scanning Electron Microscopy measurements were performed in a FEI, model Magellan, Field Gun Emission (FEG) scanning electron microscope, located in the Metrology of Materials Division (Dimat) of the Institute for Metrology, Quality and Technology (INMETRO), Duque de Caxias, RJ, Brazil. Atomic Force Microscopy measurements were perform in a Nanosurf atomic force microscope with Nanosurf easyscan controller and antivibratory table Isostage, located in the 'Complexo Multiusuário de Bioeficiência e Sustentabilidade da Pecuária da Empresa Brasileira de Pesquisa Agropecuária (EMBRAPA) Gado de Leite', Juiz de Fora, MG, Brazil.

2.3. Synthesis of gold nanorods (AuNRs)

AuNRs were prepared accordingly to a previously reported procedure [26]. Briefly, the first step consisted in the preparation of a seed suspension from the addition of a CTAB solution (5.00 mL, 0.20 mol L^{-1}) to $HAuCl_4$ (5.00 mL, 0.00050 mol L^{-1}) solution. After this, 0.60 mL of 0.010 mol L^{-1} $NaBH_4$ was added under vigorous stirring for 2 min in an ice bath and left warm up to room temperature for up to 30 min before use. A growth solution was prepared as following: CTAB (5.00 mL, 0.20 mol L^{-1}) was added to an $AgNO_3$ (0.15 mL, 0.0040 mol L^{-1}). After this, $HAuCl_4$ (5.00 mL, 0.0010 mol L^{-1}) and ascorbic acid (0.070 mL; 0.07888 mol L^{-1}) were added. Finally, 0.012 mL of *seed* was added to the growth solution at 27.0 °C, controlled with an ultrathermostatic bath. After almost 20 min, the color changed from colorless to purple. The reaction was maintained for 12 h. The resulting color of the solution remained purple. Next, in order to remove the excess of CTAB, AuNRs were centrifuged (10,244 rcf for 30 min) and redispersed in deionized water, repeating this procedure three times.

2.4. Adsorption of AuNRs on glass slides

The immobilization procedure was adapted from Fan and Brolo [27]. Glass slides were cleaned sequentially with ethanol, acetone, deionized water, and piranha solution (H_2O_2/H_2SO_4 1:4; CAUTION: this solution is strongly oxidizing and may be very harmful in the presence of metallic or organic impurities) and finally, deionized water again. After, the slides were immersed in an ethanolic MPTMS solution (10 mmol L^{-1}) for 24 h, keeping at 60 °C during the initial 2 h and at room temperature for the next 22 h. Then, the glass slides were cleaned with ethanol to remove any excess of MPTMS, immediately followed by cleaning with deionized water, an essential procedure to guarantee the removal of excess unreacted reagents. The cleaning procedure was followed by curing at 120 °C for 2 h in an oven, in order to increase the polymerization degree of the glass-bound MPTMS [28], thus improving the AuNRs adsorption. Following, the glass slides were immersed in AuNRs suspension for 24 h. The adsorption of the AuNRs during the whole procedure was followed by UV–visible spectroscopy (see Figure S1). In order to increase the number of AuNRs adsorbed, a solution of 300 μL of MPTMS and 250 μL HCl (0.1 mol L^{-1}) in 25.0 mL of deionized water was prepared, stirred for at least 1 h before silane deposition. The resulting substrate with one cycle of adsorption was immersed in this solution for about 20 min, then washed with deionized water, followed by immersion in the AuNRs suspension for 1 h, and washed again with deionized water. This procedure results in one additional cycle deposition and was performed several times until achieving an intense LSPR band for the measurements. The results presented in Figure S1 suggested that 5 cycles of deposition are enough to perform the LSPR sensitivity measurements.

2.5. Sensitivity

The sensitivity was evaluated by acquiring UV–Vis spectra of the nanoparticles in solutions with different refractive indexes. For S–P-AuNRs, during the third centrifugation cycle, the deionized water was replaced by solutions with different concentration of glycerol (from 0% up to 50% v/v) for the redispersion of the nanoparticles. The different concentrations of glycerol resulted in refractive index ranging from 1.3310 to 1.4071 RIU (refractive index unit). In the case of AuNRs-chip, they were immersed in glucose solutions with different concentrations (from 6% to 30% (m/v)), resulting in refractive index ranging from 1.3390 to 1.3465 RIU.

2.6. LSPR detection of Anti-BSA

The procedure for detection of anti-BSA consists of four steps. AuNRs-chip was immersed in an ethanolic solution of MUA 1.0 mmol L^{-1} for 72 h (MUA was used due to the formation of the well-known Au–S bond, replacing CTAB bilayer on AuNRs surface [29]), and then washed with ethanol, followed by deionized water, and immersed again in a 1:1 solution of EDC/NHS 0.10 mol L^{-1} for 3 h. After the last step, AuNRs-chip was submerged in BSA (6.6 mg L^{-1}) in phosphate buffer solution (PBS, pH = 7.52) for 6 h. In order to modify with anti-BSA, a 1.0 mg mL^{-1} anti-BSA in PBS was used; the AuNRs-chip was immersed in this solution for 12 h. The consecutive modification steps were monitored by UV–Visible spectroscopy [30].

A method adapted from Cao [29] was used to obtain the S–P-AuNRs biosensor. Initially, 5.0 mL of AuNRs suspension were added to 2.0 mL of a 20 mmol L^{-1} MUA (solubilized in alkaline aqueous solution) under vigorous stirring for 24 h. Next, the sample was centrifuged (9,641 rcf, 20 min) to remove the excess of MUA, following by redispersion in PBS. Next, 20 μL of a fresh EDC (0.10 mmol L^{-1})/NHS (0.20 mmol L^{-1}) solution was added and this suspension was vortexed for 25 min; then, 50 μL of BSA (1.0 mg mL^{-1}) in PBS was added to the suspension and vortexed for 1 h. Subsequently the suspension was centrifuged (9,641 rcf, 20 min) to remove BSA excess. In the last step, toward anti-BSA detection, 50 μL of anti-BSA (1.0 mg mL^{-1} in PBS) was added, the anti-BSA concentration were 0.1, 0.5 or 1.0 mg mL^{-1} on the experiment of the influence of the concentration, added successively. All AuNRs modification steps were monitored by UV–Vis spectroscopy.

3. Results and discussion

3.1. Characterization of solution-phase AuNRs

Fig. 1A shows a typical UV–Vis spectrum of AuNRs, which exhibit two extinction bands in the visible region due to the split of surface plasmon resonance into two distinct modes as result of the surface curvature and geometry of the nanorods [4]. The band at 510 nm is assigned to a transversal plasmon mode of the AuNRs, and the band at 750 nm is attributed to a longitudinal plasmon mode [26]. Fig. 1B shows the SEM image of AuNRs. As one can observe, the methodology used for the synthesis of AuNRs allowed to obtain a very reasonable homogeneity in shape and size. A size distribution histogram was constructed from SEM images by measuring the longitudinal and transversal dimensions of 120 AuNRs (Fig. 1C). The average longitudinal and transversal length of AuNRs was 50.7 ± 7.0 nm and 18.5 ± 3.2 nm, respectively, resulting in an aspect ratio of 2.7 ± 0.6. Additional typical SEM micrographs of the synthesized AuNRs may be found in Figure S7 of the SI file.

CTAB is an essential component in the preparation of AuNRs, the long chain helps to generate non-spherical particles, in addition to

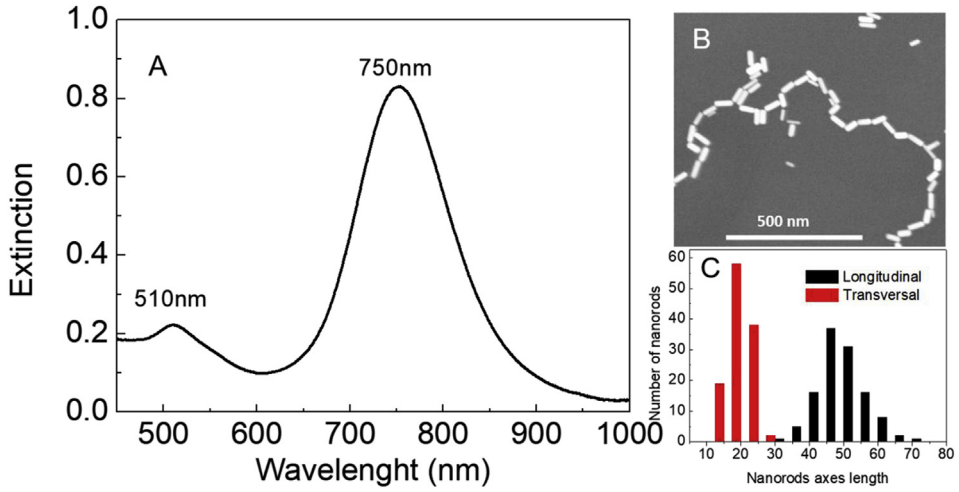

Fig. 1. Characterization of AuNRs. A) UV–Vis spectrum. B) SEM image. C) Size distribution histogram from SEM images with the longitudinal and transversal dimensions of 120 AuNRs.

interact strongly with the AuNRs surface. However, the excess of CTAB in the suspension of as-prepared AuNRs induces a redshift in the AuNRs LSPR band, due to the influence of CTAB in refractive index near the AuNRs surface. Therefore, the CTAB excess was removed before surface modification (see Figure S3).

3.2. Characterization of AuNRs-chip

The UV–Vis spectra obtained for one, five and ten cycles of AuNRs deposition on glass slides are shown in Fig. 2. It is observed the raise of characteristic AuNRs LSPR bands with the increase of the number of deposition steps. In the first cycle, one can observe a low intensity band at 680 nm, indicating the AuNRs immobilization. The intensity of this band increases with the cycles of AuNRs deposition. After 5 cycles, the LSPR signal of the AuNRs modified glass slide became similar to LSPR signal of AuNRs in suspension; finally, after 10 cycles of AuNRs deposition, both transversal and longitudinal band shows up with higher intensity. It could be inferred from this result that the substrates with 5 cycles of AuNRs deposition present intense enough LSPR bands to allow their use as biosensors; the use of AuNRs-chip assembled with 10 cycles of deposition may improve the performance, but with a considerable increase in preparation time, and the time/performance relation should be taken into account when choosing the best sensing substrate. Therefore, 5 cycles of AuNRs deposition was chosen to evaluate the sensing performance of the materials.

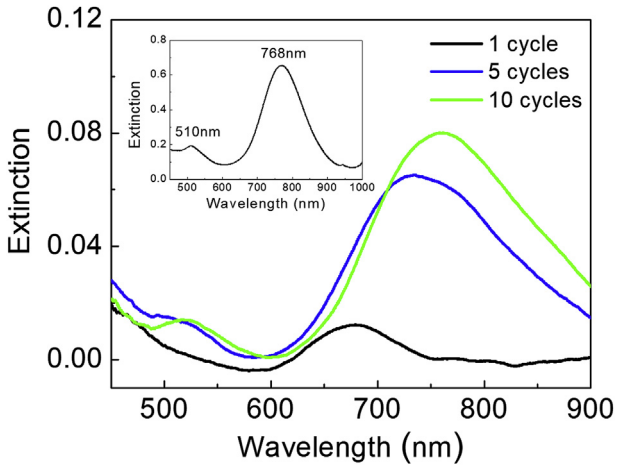

Fig. 2. UV–Vis spectra of AuNRs-chip after one, five and ten cycles of AuNRs deposition. Insert: UV–Vis spectrum of AuNRs in suspension used for the deposition cycles.

The LSPR band in the first cycle of adsorption for the AuNRs-chip is blue shifted relative to AuNRs in suspension. One should keep in mind that UV–Vis spectra of the AuNRs immobilized on glass are obtained in air, and the spectrum for AuNRs in aqueous suspension; additionally, changes in the refractive index may happen due to the removal of the excess of CTAB from the AuNRs suspension. The additional AuNRs layer deposition results in red-shifts and broadening of the LSPR bands; this fact is a result of the high sensitivity of the plasmon coupling between two particles with the interparticle separation as predicted by Maxwell-Garnet theory. A red-shift of the LSPR band position has been experimentally and theoretically associated with a decrease in interparticle distance. In fact, AFM images (Figure S2) suggest the formation of aggregates of AuNRs in samples with 5 AuNRs deposition cycles compared to samples with 1 deposition cycle, thus indicating a decrease in interparticle distance. Comparing to nanospheres, this observation would suggest an approximated value for the interparticle distance in the order of $d < 5R$, where d is the interparticle distance and R is the size of the particle [31,32].

3.3. Sensitivity

The energy of the LSPR propagation decreases when the dielectric constant of the medium (ε) or the refraction index (n) increases, as $\varepsilon = n^2$ [31]. This behavior is crucial for the application of plasmonic materials in biosensors and allows to obtain the sensitivity of the plasmonic extinction band ($\Delta\lambda_{max}$) to changes in the medium refractive index (bulk sensitivity). The sensitivity is found through the slope of a linear regression of λ_{max} *vs* refractive index, and therefore is given in nanometers per refractive index unit (nm RIU^{-1}) [33]. In order to compare the performance of the AuNRs in two different configurations, the sensitivity was obtained for both configurations AuNRs-chip and S–P-AuNRs.

Fig. 3A shows the extinction spectra of AuNRs redispersed in glycerol aqueous solution with different concentrations and refractive indexes ranging from 1.3310 to 1.4071 RIU. The sensitivity is expected to be higher for plasmonic modes with lower energy of propagation [33], therefore, the longitudinal plasmon band was chosen to characterize the changes in λ_{max} with the refractive index.

One may observe in Fig. 3A and B shows a redshift of the longitudinal LSPR band with the solution refractive index. Fig. 3C and D shows respectively the corresponding linear regression for the maximum extinction as function of the refractive index for both configurations. For S–P-AuNRs, the fitted slope was 196, corresponding to the sensitivity in nm RIU^{-1}. The measured sensitivity is in accordance to the literature, but is indicated an improvement in sensitivity relative to most of the previous reports [7]. The figure of merit (FOM), equal to sensitivity divided by the full width at half maximum (FWHM), was evaluated and the FOM observed was 2.2 RIU^{-1}. Alternatively, the sensitivity for the AuNRs-chip (five cycles of AuNRs deposition, see section 2.4) was 297 nm RIU^{-1} and FOM = 3.04 RIU^{-1}. The higher sensitivity obtained for AuNRs-chip may be assigned to the coupling between nearby nanoparticles in the film leading to an enhancement of the localized electromagnetic field, which makes the whole system more sensitive to local refractive index changes [11,34,35]. The LSPR sensitivity of AuNRs can also be improved by increasing the aspect ratio of the AuNRs, as previously experimentally and theoretically demonstrated. However, one should keep in mind that the resolution might decrease due to broadening of the absorption bandwidth, resulting from the contributions of the multipolar electron oscillations [11]. Table 1 summarizes the sensitivities and FOM achieved from AuNRs LSPR biosensors and the correlated aspect ratios. Comparing the two biosensing platforms between themselves, it may be noticed that AuNRs-chip presented larger LSPR sensitivity and FOM than previously reported biosensors based on AuNRs. Also, it is noticeable that S–P-AuNRs presented comparable sensitivity and FOM to the previous reports on AuNRs (see, for instance, reference 7), which presents aspect ratio of 2.4, sensitivity 195 nm RIU^{-1} and FOM 2.6 RIU^{-1}, quite similar to the present results. Specifically, AuNRs-chip in this study presented a sensitivity 18–75% and FOM 114–131% larger than previous reports that used AuNRs with similar aspect ratios [7,13]. Additionally, it could also be noticed that the AuNRs-chip is more user friendly than S–P-AuNRs.

3.4. LSPR detection of anti-BSA

In order to demonstrate the LSPR sensitivity of the AuNRs for the biomolecular probe/target sensing events, we have modified the AuNRs surface using a sequence of steps to obtain BSA chemically linked to the AuNRs surface, as described in the methodology (see section 2.6). Therefore, the application as biosensor has been performed by using the AuNRs-BSA as a probe. The results for S–P-AuNRs and AuNRs-chip based biosensors are presented in Fig. 4 and Table 2, respectively, and a blank experiment is presented in Figure S4.

As predicted by Gans theory [4], a redshift was observed as result of an increase in the dielectric constant due to the presence of adsorbed molecules on the AuNRs surface (Fig. 4). A total of 17 nm and 30 nm redshift was observed for S–P-AuNRs and AuNRs-chip after BSA modification, compared to bare AuNRs (Table 2). Concerning the anti-BSA detection, one can observe an additional redshift average of 2.8 and 2.9 nm, respectively, relative to the BSA-modified AuNRs (Fig. 4 and Table 2). The observed red-shift of S–P-AuNRs in the presence of anti-BSA is dependent on the antibody concentration used in the experiment, as it may be found in Figure S5. The larger redshift for BSA compared to anti-BSA is related to the large size of both biomolecules, which results in a predicted large LSPR shift with adsorption of the first, due to a large change in local refractive index near the AuNRs surface, but also resulting in available interaction centers for the antibody far from gold surface, so that the interacting anti-BSA is expected to be few nanometers from surface, which significantly decrease the influence on the local refractive index by the antibody, resulting in lower sensitivity compared to BSA. The measurement errors reported in Table 2 are related to the standard deviation of four and six measurements of S–P-AuNRs and AuNRs-chip (on different spots), respectively. The larger error in the LSPR shift associated to AuNRs-chip in Anti-BSA detection is related to the heterogeneity of the biosensor. AuNRs-chip are more heterogeneous than S–P-AuNRs

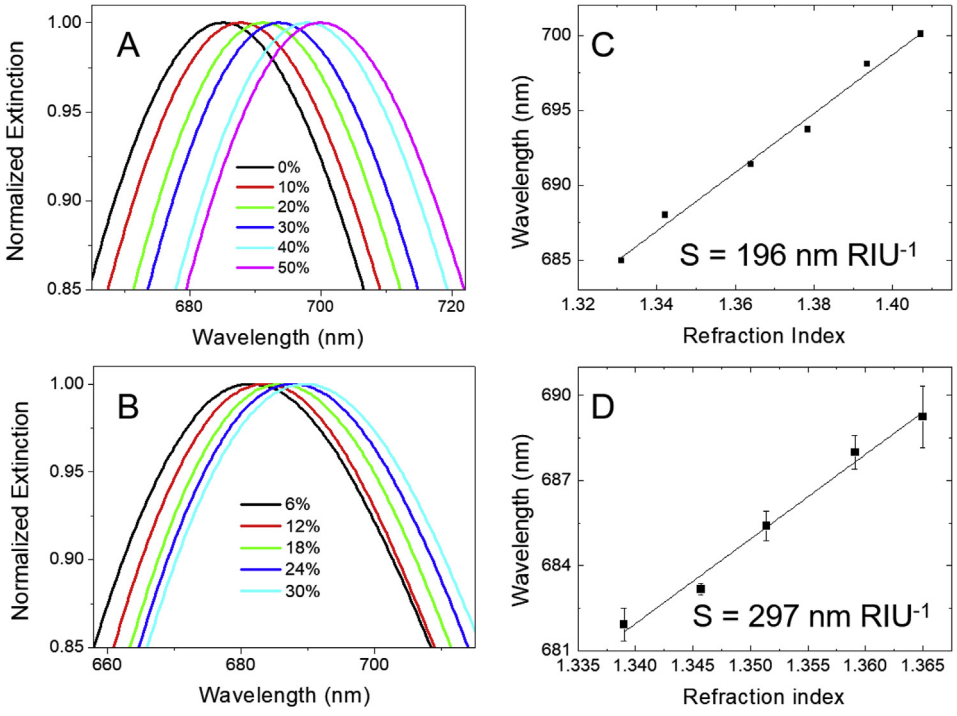

Fig. 3. Measurement of sensitivity of AuNRs. UV–Vis spectra of A) solution-phase AuNRs in glycerol solutions with different concentrations and B) AuNRs-chip in glucose solutions with different concentrations. Sensitivity curve for C) solution-phase AuNRs and D) AuNRs-chip.

Table 1
Competitive aspect ratio, LSPR sensitivity and FOM for AuNRs based LSPR biosensors reported in literature.

Material	Aspect ratio	Sensitivity (nm RIU^{-1})	FOM (RIU^{-1})	Sensitivity improvement[a]	FOM improvement[b]	Reference
AuNRs on glass slides	2.7	297	3.0	–	–	This work
AuNRs in suspension	2.7	196	2.2	–	–	This work
AuNRs on glass slides	2.2	252	n.i.[c]	18%	–	[36]
AuNRs on glass slides	3.3	170	1.3	75%	131%	[13]
AuNRs on glass slides	5.2	366	n.i.[c]	–	–	[14]
AuNRs on glass slides	3.5	330	1.4	–	114%	[37]

[a] Percent improvement of the LSPR sensitivity of AuNRs-chip developed in this work compared to the cited studies.
[b] Percent improvement of the LSPR FOM of AuNRs-chip developed in the present study compared to the literature.
[c] n.i. = not informed.

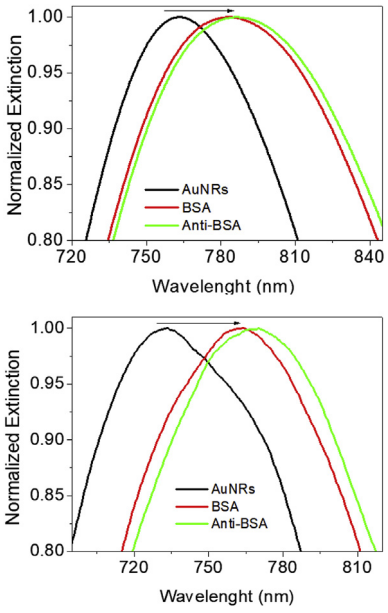

Fig. 4. UV–Vis spectra to monitor the BSA-*anti*-BSA bio-binding. A) S–P-AuNRs. B) AuNRs-chip.

because of the formation of aggregates as the number of deposition increase, consequently increasing the broadening of LSPR band, as explained in section 3.2; the increase in the aggregation of AuNRs was observed using AFM imaging, presented in in Figure S2. The LOD (limit of detection) was calculated considering the AuNRs-BSA as blank for the anti-BSA detection in the equation $LOD = 3\sigma_B/S$, where σ_B is the standard deviation from the blank and S is the sensitivity). It is important to highlight that the LSPR bands for both configurations have not suffered any significant changes in position, increase in width, substantial shifts or loss of intensity after all surface changes in the present study; therefore, both configurations remained stable during the modification processes.

Although both configurations for the biosensor are based on the same material, the results show that vicinity and environment affect the biosensor performance. AuNRs-chip presented higher sensitivity, FOM and lower LOD. The better performance of AuNRs-chip is assigned to an enhanced electromagnetic field resulted from the coupling between the AuNRs in the film, allowed by the proximity between these particles evidenced with AFM and UV–Vis data.

Concerning the red-shift and LOD for Anti-BSA detection, similar values were obtained, however, one should keep in mind that S–P-AuNRs have a larger surface area available for antigen-antibody interaction than the AuNRs-chip (3D against a 2D configuration), essentially because immobilized AuNRs would have at least one side of the surface adsorbed on glass. Taking into account the gold unit cell volume, AuNR volume and area in addition to the area of AuNR film, a rough estimate for the AuNRs available for biomolecules immobilization was found to be 10^3 fold larger for S–P-AuNRs than AuNRs-chip biosensor. This fact wasn't observed on BSA modification, due to BSA concentration was *ca.* 6 times lager in AuNRs-chip modification. In fact, the LSPR band of S–P-AuNRs is considerably more intense than AuNRs-chip (Figure S6). Additionally, according to Equation (1), where $\Delta\lambda_{max}$ is the LSPR shift, *S* is the sensitivity, n_{ads} and n_{med} are, respectively, the refractive indices of the adsorbate (proteins) and medium (water) surrounding the nanoparticle, *d* is the effective thickness of the adsorbate layer and I_d is the electromagnetic-field decay length from the LSPR [38], a higher surface coverage, which is expected to increase n_{ads}, is expected to increase the LSPR shift.

$$\Delta\lambda_{max} = S(n_{ads} - n_{med})\left(1 - e^{-2d/I_d}\right) \quad (1)$$

4. Conclusions

AuNRs with good homogeneity of shape and size were successfully applied as a label-free LSPR biosensor, reaching sensitivities and FOM expressively higher than others AuNRs based sensors. The sensitivity was found to be dependent of the configuration used to assemble the biosensor, S–P-AuNRs and AuNRs-chip presented LSPR sensitivities of 196 and 297 nm RIU^{-1} and FOM of 2.2 RIU^{-1} and 3.0 RIU^{-1}, respectively. These differences were assigned to the enhanced electromagnetic field in the AuNRs-chip resulted from the coupling of these nanoparticles in the film. However, concerning the biodetection, this difference became not significant. Another advantage of this configuration is being user friendly. It should be noticed that the presented results are motivating, so that more experiments on the development of the presented biosensing platforms would be important to optimize biosensor specificity; however, the results presented here are

Table 2
LSPR average red-shifts and their standard deviation for each surface modification on AuNRs surface.

Material	AuNRs – BSA shift (nm)	AuNRs – Anti-BSA shift (nm)	$\Delta\lambda_{max}$ Anti-BSA detection (nm)	LOD RIU
S–P-AuNRs	17.19 ± 4.20	19.94 ± 4.68	2.76 ± 0.58	0.064
AuNRs-chip	30.25 ± 5.39	33.09 ± 6.56	2.85 ± 2.41	0.054

indicative that such efforts would be potentially beneficial for the development of the immobilized AuNRs family of biosensors. Finally, both substrates were stable after surfaces modifications (evaluated by UV–Vis spectroscopy) used to construct the chemical platform for biomolecular recognition in the BSA/anti-BSA antigen/antibody system.

Declaration of competing interest

The authors declare that they have no known competing financial interests or personal relationships that could have appeared to influence the work reported in this paper.

Acknowledgements

The authors thank Fundação de Amparo a Pesquisa do Estado de Minas Gerais, Brazil, FAPEMIG (CEX-APQ-01283/14), Conselho Nacional de Desenvolvimento Científico e Tecnológico, Brazil, CNPq (303439/2015-7 and 423244/2016-7), Coordenação de Aperfeiçoamento de Pessoal de Nível Superiror, Brazil, CAPES (financing code 001), and Fundação de Amparo a Pesquisa do Estado do Rio Grande do Sul, Brazil, FAPERGS for financial support. Dr. Bráulio S. Archanjo, from Divisão de Metrologia de Materiais (Dimat) of the Instituto Nacional de Metrologia, Qualidade e Tecnologia (INMETRO) for access to Scanning Electron Microscopy facilities, Dr. Humberto de Mello Brandão from Complexo Multiusuário de Bioeficiência e Sustentabilidade da Pecuária da Empresa Brasileira de Pesquisa Agropecuária (EMBRAPA) Gado de Leite for access to Atomic Force Microscopy facilities, and M.Sc. Moyra Freitas Vieira for carrying out the AFM measurements. LPFP thanks CAPES for a fellowship. GFSA and JFLS thank CNPq for research fellowships.

Appendix A. Supplementary data

Supplementary data to this article can be found online at https://doi.org/10.1016/j.aca.2019.07.032.

References

[1] J. Langer, S.M. Novikov, L.M. Liz-Marzan, Sensing using plasmonic nanostructures and nanoparticles, Nanotechnology (2015) 26.
[2] Y.Y. Wang, J.H. Zhou, J.H. Li, Construction of plasmonic nano-biosensor-based devices for point-of-care testing, Small Methods 1 (2017).
[3] A.-I. Henry, J.M. Bingham, E. Ringe, L.D. Marks, G.C. Schatz, R.P. Van Duyne, Correlated structure and optical property studies of plasmonic nanoparticles, J. Phys. Chem. C 115 (2011) 9291–9305.
[4] J. Cao, T. Sun, K.T.V. Grattan, Gold nanorod-based localized surface plasmon resonance biosensors: a review, Sens. Actuators B Chem. 195 (2014) 332–351.
[5] E. Petryayeva, U.J. Krull, Localized surface plasmon resonance: nanostructures, bioassays and biosensing—a review, Anal. Chim. Acta 706 (2011) 8–24.
[6] P.D. Howes, R. Chandrawati, M.M. Stevens, Colloidal nanoparticles as advanced biological sensors, Science (2014) 346.
[7] H. Chen, X. Kou, Z. Yang, W. Ni, J. Wang, Shape- and size-dependent refractive index sensitivity of gold nanoparticles, Langmuir 24 (2008) 5233–5237.
[8] M.C. Estevez, M.A. Otte, B. Sepulveda, L.M. Lechuga, Trends and challenges of refractometric nanoplasmonic biosensors: a review, Anal. Chim. Acta 806 (2014) 55–73.
[9] C.M. Cobley, J. Chen, E.C. Cho, L.V. Wang, Y. Xia, Gold nanostructures: a class of multifunctional materials for biomedical applications, Chem. Soc. Rev. 40 (2011) 44–56.
[10] P.L. Truong, B.W. Kim, S.J. Sim, Rational aspect ratio and suitable antibody coverage of gold nanorod for ultra-sensitive detection of a cancer biomarker, Lab Chip 12 (2012) 1102–1109.
[11] H. Huang, C. Tang, Y. Zeng, X. Yu, B. Liao, X. Xia, P. Yi, P.K. Chu, Label-free optical biosensor based on localized surface plasmon resonance of immobilized gold nanorods, Colloids Surfaces B Biointerfaces 71 (2009) 96–101.
[12] M. Potara, A.-M. Gabudean, S. Astilean, Solution-phase, dual LSPR-SERS plasmonic sensors of high sensitivity and stability based on chitosan-coated anisotropic silver nanoparticles, J. Mater. Chem. 21 (2011) 3625–3633.
[13] K.M. Mayer, S. Lee, H. Liao, B.C. Rostro, A. Fuentes, P.T. Scully, C.L. Nehl, J.H. Hafner, A label-free immunoassay based upon localized surface plasmon resonance of gold nanorods, ACS Nano 2 (2008) 687–692.
[14] C.-D. Chen, S.-F. Cheng, L.-K. Chau, C.R.C. Wang, Sensing capability of the localized surface plasmon resonance of gold nanorods, Biosens. Bioelectron. 22 (2007) 926–932.
[15] J.-F. Masson, Surface plasmon resonance clinical biosensors for medical diagnostics, ACS Sens. 2 (2017) 16–30.
[16] J. Ferreira, M.J.L. Santos, M.M. Rahman, A.G. Brolo, R. Gordon, D. Sinton, E.M. Girotto, Attomolar protein detection using in-hole surface plasmon resonance, J. Am. Chem. Soc. 131 (2009), 436-+.
[17] G.A. Lopez, M.C. Estevez, M. Soler, L.M. Lechuga, Recent advances in nanoplasmonic biosensors: applications and lab-on-a-chip integration, Nanophotonics 6 (2017) 123–136.
[18] F. Della Pelle, A. Scroccarello, S. Scarano, D. Compagnone, Silver nanoparticles-based plasmonic assay for the determination of sugar content in food matrices, Anal. Chim. Acta 1051 (2019) 129–137.
[19] M.T. Alula, L. Karamchand, N.R. Hendricks, J.M. Blackburn, Citrate-capped silver nanoparticles as a probe for sensitive and selective colorimetric and spectrophotometric sensing of creatinine in human urine, Anal. Chim. Acta 1007 (2018) 40–49.
[20] Y. Wang, Y. Zeng, W.S. Fu, P. Zhang, L. Li, C.Y. Ye, L. Yu, X.C. Zhu, S. Zhao, Seed-mediated growth of Au@Ag core-shell nanorods for the detection of ellagic acid in whitening cosmetics, Anal. Chim. Acta 1002 (2018) 97–104.
[21] J.L. Hammond, N. Bhalla, S.D. Rafiee, P. Estrela, Localized surface plasmon resonance as a biosensing platform for developing countries, Biosensors 4 (2014) 172–188.
[22] A.G. Brolo, Plasmonics for future biosensors, Nat. Photonics 6 (2012) 709–713.
[23] M.-Y. Pan, K.-L. Lee, S.-C. Lo, P.-K. Wei, Resonant position tracking method for smartphone-based surface plasmon sensor, Anal. Chim. Acta 1032 (2018) 99–106.
[24] M.-Y. Pan, K.-L. Lee, L. Wang, P.-K. Wei, Chip-based digital surface plasmon resonance sensing platform for ultrasensitive biomolecular detection, Biosens. Bioelectron. 91 (2017) 580–587.
[25] M. Veiseh, M.H. Zareie, M. Zhang, Highly selective protein patterning on Gold–Silicon substrates for biosensor applications, Langmuir 18 (2002) 6671–6678.
[26] B. Nikoobakht, M.A. El-Sayed, Preparation and growth mechanism of gold nanorods (NRs) using seed-mediated growth method, Chem. Mater. 15 (2003) 1957–1962.
[27] M. Fan, A.G. Brolo, Silver nanoparticles self assembly as SERS substrates with near single molecule detection limit, Phys. Chem. Chem. Phys. 11 (2009) 7381–7389.
[28] M.E. Marques, A.A.P. Mansur, H.S. Mansur, Chemical functionalization of surfaces for building three-dimensional engineered biosensors, Appl. Surf. Sci. 275 (2013) 347–360.
[29] J. Cao, E.K. Galbraith, T. Sun, K.T.V. Grattan, Effective surface modification of gold nanorods for localized surface plasmon resonance-based biosensors, Sens. Actuators B Chem. 169 (2012) 360–367.
[30] J.P. Monteiro, J. Ferreira, R.G. Sabat, P. Rochon, M.J.L. Santos, E.M. Girotto, SPR based biosensor using surface relief grating in transmission mode, Sens. Actuators B Chem. 174 (2012) 270–273.
[31] J.F.L. Santos, M.J.L. Santos, A. Thesing, F. Tavares, J. Griep, M.R.F. Rodrigues, Localized surface plasmon ressonance applied to biosensors and solar cells, Quim. Nova 39 (2016) 1098–1111.
[32] A. Thesing, L.F. Loguercio, M.J.L. Santos, J. Ferreira, Simple approach to obtain a localized surface plasmon resonance sensor based on poly(dimethylsiloxane)/gold nanoparticles nanocomposite, J. Nanosci. Nanotechnol. 16 (2016) 10080–10086.
[33] J.P. Monteiro, L.B. Carneiro, M.M. Rahman, A.G. Brolo, M.J.L. Santos, J. Ferreira, E.M. Girotto, Effect of periodicity on the performance of surface plasmon resonance sensors based on subwavelength nanohole arrays, Sens. Actuators B Chem. 178 (2013) 366–370.
[34] A.L.C.M.d. Silva, M.G. Gutierres, A. Thesing, R.M. Lattuada, J. Ferreira, SPR biosensors based on gold and silver nanoparticle multilayer films, J. Braz. Chem. Soc. 25 (2014) 928–934.
[35] L. Vigderman, B.P. Khanal, E.R. Zubarev, Functional gold nanorods: synthesis, self-assembly, and sensing applications, Adv. Mater. 24 (2012) 4811–4841.
[36] S.M. Marinakos, S. Chen, A. Chilkoti, Plasmonic detection of a model analyte in serum by a gold nanorod sensor, Anal. Chem. 79 (2007) 5278–5283.
[37] J.-H. Pai, C.-T. Yang, H.-Y. Hsu, A.B. Wedding, B. Thierry, Development of a simplified approach for the fabrication of localised surface plasmon resonance sensors based on gold nanorods functionalized using mixed polyethylene glycol layers, Anal. Chim. Acta 974 (2017) 87–92.
[38] S. Zhai, H. Zhao, Enhancement of sensitivity of the solution-phase localized surface plasmon by a nanostructured substrate, MRS Advances 1 (2016) 2059–2064.